Published in final edited form as:
J Mol Med (Berl). 2014 May ; 92(5): 473–485. doi:10.1007/s00109-014-1120-y.

Control of Autophagy Maturation by Acid Sphingomyelinase in Mouse Coronary Arterial Smooth Muscle Cells: Protective Role in Atherosclerosis

Xiang Li, **Ming Xu**, **Ashley L. Pitzer**, **Min Xia**, **Krishna M. Boini**, **Pin-Lan Li**, and **Yang Zhang**
Department of Pharmacology & Toxicology, School of Medicine, Virginia Commonwealth University, Richmond, VA 23298, USA

Abstract

Recent studies have indicated a protective role of autophagy in regulating vascular smooth muscle cells homeostasis in atherogenesis, but the mechanisms controlling autophagy, particularly autophagy maturation, are poorly understood. Here, we investigated whether acid sphingomyelinase (ASM)-regulated lysosome function is involved in autophagy maturation in coronary arterial smooth muscle cells (CASMCs) in the pathogenesis of atherosclerosis. In coronary arterial wall of ASM-deficient (*Smpd1*$^{-/-}$) mice on Western diet, there were high expression levels of both LC3B, a robust marker of autophagosomes (APs), and p62, a selective autophagy substrate, compared to those in wild type (*Smpd1*$^{+/+}$) mice. By Western blotting and flow cytometry, atherogenic stimulation of *Smpd1*$^{+/+}$ CASMCs with 7-ketocholesterol was found to significantly enhance LC3B expression and increase the content of both APs and autophagolysosomes (APLs). In *Smpd1*$^{-/-}$ CASMCs, such 7-ketocholesterol-induced increases in LC3B and p62 expression and APs were further augmented, but APLs formation was abolished. Analysis of fluorescence resonance energy transfer (FRET) between fluorescence-labeled LC3B and Lamp1 (lysosome marker) showed that 7-ketocholesterol markedly induced fusion of APs with lysosomes in *Smpd1*$^{+/+}$ CASMCs, which was abolished in *Smpd1*$^{-/-}$ CASMCs. Moreover, 7-ketocholesterol-induced expression of cell dedifferentiation marker vimentin and proliferation was enhanced in *Smpd1*$^{-/-}$ CASMCs compared to those in *Smpd1*$^{+/+}$ CASMCs. Lastly, overexpression of ASM further increased APLs formation in *Smpd1*$^{+/+}$ CASMCs and restored APLs formation in *Smpd1*$^{-/-}$ CASMCs indicating that increased ASM expression is highly correlated with enhanced APLs formation. Taken together, our data suggest that the control of lysosome trafficking and fusion by ASM is essential to a normal autophagic flux in CASMCs, which implicates that the deficiency of ASM-mediated regulation of autophagy maturation may result in imbalance of arterial smooth muscle cell homeostasis and thus serve as an important atherogenic mechanism in coronary arteries.

Correspondence should be addressed to: Yang Zhang, Ph.D, Department of Pharmacology & Toxicology, Medical College of Virginia Campus, Virginia Commonwealth University, Richmond, VA 23298 Tel: (804) 828-0738, Fax: (804) 828-4794, yzhang3@vcu.edu.

Conflict of interest
None.

Keywords

Acid sphingomyelinase; autophagic flux; lysosome; coronary arterial smooth muscle cell; coronary artery; atherosclerosis

INTRODUCTION

Acid sphingomyelinase (ASM; gene symbol *Smpd1*) hydrolyzes sphingomyelin to ceramide and phosphorylcholine, preferentially at an acidic pH, which exists in at least two forms: a lysosomal ASM and a secretory ASM[1]. Both forms are derived from the same gene, but differ in their glycosylation pattern and differential processing at the NH_2-terminus[1]. For most part, ASM seems to reside in classic lysosomes, where it mediates the catabolism of sphingomyelin. A genetic defect in ASM leads to the accumulation of sphingomyelin and a lysosomal storage disorder named Niemann-Pick disease. The pooling of ASM in secretory lysosomes seems to participate in signal transduction events; however, the precise role of ASM in the development of atherosclerosis remains unclear. Secretory ASM may be atherogenic, whereas the lysosomal form of ASM may have anti-atherogenic effects[2-5]. Previous studies demonstrated that the atherogenic action of secretory ASM in the plasma may be mainly associated with ceramide-promoted lipoprotein aggregation or uptake by arterial-wall macrophages that leads to foam cell formation[5-6]. However, a recent study demonstrated that adenovirus-mediated expression and secretion of ASM into the circulation did not exacerbate but decreased lesion formation in atherosclerotic $ApoE^{-/-}$ mice, indicating that plasma ASM activity may not be determinant for plaque formation during atherogenesis[2]. In another aspect, lysosomal ASM activity can be anti-atherogenic since it increases sphingomyelin hydrolysis reducing accumulation of cholesterol in lysosome of macrophages given that sphingomyelin has high binding affinity to cholesterol[7-8]. Although these previous studies in animal models indicated that ASM signaling in atherosclerosis depends upon the isoform of this enzyme, clinical studies reported that patients of Niemann-Pick disease type A and B with a deficiency in ASM activity had high incidences of coronary atherosclerosis [9], suggesting that ASM signaling may provide protection from coronary atherogenic injury in humans. In this regard, the present study was designed to explore the protective role of ASM in arterial smooth muscle cells in the context of atherogenesis.

It has been well established that the role of arterial smooth muscle cells in atherosclerosis relates to their proliferative and secretory properties; they proliferate, grow, and migrate into the intima and produce extracellular matrix to induce fibrosis. The importance of increased smooth muscle cell proliferation in the growth of atherosclerotic plaques has been well studied in animal models as well as in human vascular obstructive lesions [10-11]. Recent studies indicate a protective role of autophagy in regulating vascular SMC homeostasis during atherogenesis. Under physiological conditions, autophagy works in a nonstop, reparative, and life-sustaining way to maintain normal cellular homeostasis[12]. In the early stage of atherogenesis, enhanced autophagy in arterial smooth muscle cells exerts beneficial effects by inducing modulation of smooth muscle cells to a more differentiated, quiescent, and contractile phenotype, thereby decreasing cell proliferation and preventing fibrosis[13].

Thus, it is important to explore the mechanisms involved in smooth muscle cell autophagy in order to prevent smooth muscle cell dysfunction induced by defective autophagy during the early stage of atherogenesis.

Autophagy is a highly regulated catabolic mechanism that eukaryotic cells use to degrade long-lived proteins and excessive or damaged organelles [14]. The autophagic process includes autophagic induction/formation of autophagosomes (APs) and autophagic flux. Autophagic flux consists of two steps: (1) lysosome trafficking and fusion with APs leading to maturation of APs to autophagolysosomes (APLs); and (2) breakdown of autophagic contents in APLs by lysosomal cathepsins [15-16]. The molecular mechanisms and regulatory pathways for the formation of APs are relatively well understood due to the discovery of mammalian autophagy genes (*Atg* genes) [16-17], but the molecular mechanisms regulating APs fusion with lysosomes are still understudied. Given the intracellular location of ASM and ceramide production in lysosomes and their signaling roles in various cellular activities, the present study hypothesized that ASM importantly controls lysosome function and thereby participates in the regulation of APs trafficking and fusion with lysosomes. To test this hypothesis, we first characterized the autophagic process including APs formation and autophagic flux in coronary arterial smooth muscle cells (CASMCs) under atherogenic stimulation *in vitro* and *in vivo*. Then, we examined whether ASM controls autophagy maturation by regulating lysosome function to traffic, or fuse, with APs to form APLs in CASMCs.

MATERIALS AND METHODS

Mice

ASM-deficient (*Smpd1*$^{-/-}$; *Smpd1* is the gene symbol for ASM gene *sphingomyelin phosphodiesterase 1*) and wild-type (*Smpd1*$^{+/+}$) mice were used in the present study as we described previously [18-19]. All experimental protocols were reviewed and approved by the Animal Care Committee of Virginia Commonwealth University. All animals were provided standard rodent chow and water ad libitum in a temperature-controlled room.

Immunofluorescent staining of coronary arteries

Eight-week-old male mice were fed 10-week normal diet or Western diet containing (g%): protein 20, carbohydrate 50, and fat 21 (Dytes, PA) as described previously [20-22]. Mice were sacrificed by cervical dislocation under ether anesthesia. The hearts with intact coronary arteries were obtained for coronary dissection or frozen in liquid nitrogen for preparation of frozen section slides. The expression of indicated proteins was detected in mouse heart frozen slides using corresponding immunofluorescence labeled antibodies as described previously [23-24]. Briefly, the tissues of hearts with coronary arteries were frozen in Tissue-Tek OCT, cut by cryostat into 10 μm sections and mounted on Superfrost/Plus slides for immunofluorescent staining. After fixation with acetone, the slides were incubated with indicated antibodies (1:50) overnight at 4°C. After incubation with primary antibodies, the slides were washed and labeled with corresponding Alexa-488 conjugated secondary antibodies (Invitrogen) used at a dilution of 1:200. The slides were then washed, mounted, and subjected to confocal microscopic analysis (Fluoview FV1000, Olympus,

Japan). Colocalization was analyzed using Image Pro Plus software (Media Cybernetics, Inc, Bethesda, MD), and the colocalization coefficient was represented by Pearson's correlation coefficient as we described [23].

Primary cell culture of mouse coronary arterial smooth muscle cells (CASMCs)

Mouse CASMCs were isolated as previously described [25]. In brief, mice were deeply anesthetized with intraperitoneal injection of pentobarbital sodium (25 mg/kg). The heart was excised with an intact aortic arch and immersed in a petri dish filled with ice-cold Krebs-Henseleit solution. A 25-gauge needle filled with Hanks' buffered saline solution was inserted into the aortic lumen opening while the whole heart remained in the ice-cold buffer solution. The opening of the needle was inserted deep into the heart close to the aortic valve. The needle was tied in place with the needle tip as close to the base of the heart as possible. The infusion pump was started with a 20 ml syringe containing warm HBSS through an intravenous extension set at a rate of 0.1 ml/min for 15 min. HBSS was replaced with warm enzyme solution (1 mg/ml collagenase type I, 0.5 mg/ml soybean trypsin inhibitor, 3% bovine serum albumin (BSA), and 2% antibiotic), which was flushed through the heart at a rate of 0.1 ml/min. Perfusion fluid was collected at 30, 60, and 90-min intervals. At 90 min, the heart was cut with scissors, and the apex was opened to flush out the cells that collected inside the ventricle. The fluid was centrifuged at 1000 rpm for 10 min, the cell-rich pellets were mixed with the media described below, and the cells were plated on 2% gelatin-coated six-well plates and incubated in 5% CO_2 at 37 °C. Advanced Dulbecco's modified Eagle's medium (DMEM) with 10% fetal bovine serum, 10% mouse serum, and 2% antibiotics were used for isolated CASMCs. The identification of CASMCs was based on positive staining by anti-α-actin antibody and the SMCs morphology. The medium was replaced 3 days after cell isolation and then once or twice each week until the cells grew to confluence. All studies were performed with cells of passage of 3-5. Six-week-old male C57BL/6J ASM-deficient (*Smpd1*$^{-/-}$) mice and their wild-type littermates (*Smpd1*$^{+/+}$) were used in the present study, and mouse genotyping was performed as we described previously [18, 26].

Western blot analysis—Western blot analysis was performed as we described previously [27]. In brief, proteins from the CASMCs were extracted using sucrose buffer (20 mM HEPES, 1mM EDTA, 255 mM sucrose, cocktail o protease inhibitors (Roche), pH 7.4). After boiling for 5 min at 95 °C in a 5× loading buffer, 30μg of total proteins were separated by a 12% sodium dodecyl sulfate-polyacrylamide gel electrophoresis (SDS-PAGE). The proteins of these samples were then electrophoretically transferred at 100 V for 1 hour onto a PVDF membrane (Bio-Rad, USA). The membrane was blocked with 5% nonfat milk in Tris-buffered saline-Tween 20. After washing, the membrane was probed with 1:1000 dilution of primary mouse or rabbit antibodies against LC3B (Cell signaling), p62 (Cell signaling), vimentin (Santa Cruz), or β-actin (Santa Cruz) overnight at 4 °C followed by incubation with horseradish peroxidase-labeled IgG (1:5000). The immuno-reactive bands were detected by chemiluminescence methods and visualized on Kodak Omat X-ray films. Densitometric analysis of the images obtained from X-ray films was performed using the Image J software (NIH).

Flow cytometric detection of autophagolysosomes (APLs) formation

The APLs formation was analyzed by flow cytometry using a lysomotrophic dye, acridine orange [28]. Acridine orange accumulates in acidic vesicles, such as lysosomes, to display red fluorescence, but is green fluorescent in neutral environments, such as in the cytosol and nuclei. Since APLs are larger acidic compartments compared to lysosomes, fusion of lysosomes with APs to form APLs will result in an increase of the red-to-green fluorescence intensity ratio. Briefly, cells were stained with acridine orange (2 g/mL) for 17 min and washed twice in phenol red-free RPMI 1640 with 2% FBS. Then the intensity ratio of red-to-green fluorescence of cells was obtained by flow cytometry.

Flow cytometric analysis of autophagosomes (APs)

Autophagic vacuoles including APs and APLs in cells, were detected using a CytoID Autophagy Detection Kit (Enzo, PA, USA) following manufacturer's instruction. The CytoID fluorescent reagents specifically detect the autophagic vacuoles formed during autophagy. Briefly, cells were trypsinized, spun down, and washed twice in phenol red-free RPMI 1640 with 2% fetal bovine serum (FBS). The cells were resuspended in 0.5 ml of freshly diluted CytoID reagents and incubated at 37 °C for 30 min. The CytoID fluorescence of cells was immediately analyzed by flow cytometry using a flow cytometer (GUAVA, Hayward, CA, USA). The percentage of cells with CytoID staining was used to represent the dynamic balance between AP formation and its degradation via autophagic flux. By combining with an inhibitor of lysosomal degradation (chloroquine, 300 μM) that inhibits autophagic flux, the CytoID assay can be used to determine whether the autophagic vacuole accumulation is due to decrease in autophagic flux.

Confocal Microscopic and Fluorescence Resonance Energy Transfer (FRET) Analysis

For confocal analysis, cultured CASMCs were grown on glass coverslips, stimulated or unstimulated, fixed in 4% paraformaldehyde in phosphate-buffer saline (PFA/PBS) for 15 min as described [29]. After being permeablized with 0.1% Triton X-100/PBS and rinsed with PBS, the cells were incubated overnight at 4 °C with indicated primary antibodies: rat anti-Lamp1 (1:200, BD Biosciences), or rabbit anti-LC3B (1:200, Cell Signaling). After washing, these slides were incubated with either Alexa-488- or Alexa-555-labeled secondary antibodies for 1 h at room temperature. The slides were mounted and subjected to examinations using a confocal laser scanning microscope (Fluoview FV1000, Olympus, Japan). The lysosome number per cells was quantified by analyzing Alexa-Lamp1-positive particles using Image J software (NIH). An acceptor bleaching protocol was used to measure the FRET efficiency between Alexa488-Lamp1/Alexa555-LC3B as described previously [19, 30]. Briefly, after the pre-bleaching image was normally taken, the laser intensity at the excitement wavelength of the acceptor (Alexa555) was increased from 50 to 98% and continued to excite the cell sample for 2 min to bleach the acceptor fluorescence. After the intensity of the excitement laser for acceptor was adjusted back to 50%, the post-bleaching image was taken for Alexa488. A FRET image was obtained by subtraction of the pre-bleaching images from the post-bleaching images and given a dark blue color. After measuring Alexa488 fluorescence intensity of the pre-, post-, and FRET images, the FRET

efficiency was calculated through the following equation: $E = (Alexa488_{post} - Alexa488_{pre})/Alexa488_{post} \times 100\%$.

ASM activity assay

The enzymatic hydrolysis of sphingomyelin to ceramide and phosphocholine by sphingomyelinase was measured at pH 5.0 with the Amplex® Red reaction kit (Invitrogen) according to manufacturer's instructions with minor modifications. Briefly, cells (5×10^5) were pelleted by centrifugation at 1,000× *g* for 10 min at 4°C and washed twice with ice-cold PBS. Cells were washed with PBS three times, and the pellet was resuspended in 0.2 ml of lysis buffer containing 1% Triton X-100, 1× proteinase inhibitor cocktail (Roche), 1 mM EDTA, and 50 mM sodium acetate (pH 5.0) for 60 min on ice. The lysates were subjected to centrifugation at 17,000 *g* for 10 min at 4°C to remove nuclei and unbroken cells. The protein concentration in the supernatant fraction was measured with the Bio-Rad protein assay. Acid sphingomyelinase activity in the supernatant fractions was assayed in a two-step reaction system. First, 20 μg proteins of supernatant fraction were incubated with 0.5 mM sphingomyelin to generate phosphocholine and ceramide at pH of 5.0 for 60 min at 37°C. The reaction was then placed on ice and mixed with same volume of Amplex® Red reagent solution, which contains 10 μM Amplex® Red reagent, 2 U/ml horseradish peroxidase, 0.2 U/ml choline oxidase, 8 U/ml alkaline phosphatase and 100 mM Tris-HCl (pH 8.0). This reaction mixture was further incubated at 37°C for 60 min to allow alkaline phosphatase hydrolysis of phosphocholine to choline, which is oxidized by choline oxidase to generate betaine and H_2O_2. H_2O_2 in the presence of horseradish peroxidase reacts with Amplex® Red to generate the fluorescent resorufin. Fluorescence intensity was measured at excitation and emission wavelengths of 545 and 590 nm, respectively. The enzyme activity of ASM in the protein lysates was normalized to activity (U) of sphingomyelinase from *Bacillus cereus* (provided as a control within the kit). One unit is defined as the amount of sphingomyelinase that will hydrolyse 1 μmole of TNPAL–sphingomyelin per minute at pH 7.4 at 37°C.

Assays for lysosomal cathepsin activity

The catalytic activities of cathepsin B (Abcam) and cathepsin D (Sigma) were determined using commercially available kits following manufacturer's instructions. For each assay, 20 -50 μg of cell lysates were assayed in a 96-well plate using an internally quenched fluorescent substrate for cathepsin B or D. The plates were incubated at 37°C and fluorescent values were determined at 10 min intervals using a fluorescent microplate reader (BioTek, Flx800). Values measured within the linear range of the reaction were used for the calculations.

Proliferation assay

The proliferation of CASMCs was quantified using a Aqueous One Solution Cell Proliferation Assay kit (Promega) following the manufacturer's instruction as we previously described [13]. Cells were cultured in a 96-well plate (2, 000 cells per well) with or without treatment as indicated. After 48 hours, cells were incubated with 20 L Aqueous One Solution for 60 min at 37°C. Then the absorbance (at 490 nm) of each sample was measured using a microplate reader. Calibration curves showed the fluorescence reading to be

proportional to the cell number. The proliferation rate was obtained by calculating the fold change in the cell number of each sample before and after 48-hour incubation.

Nucleofection

Transfection of cDNA plasmids was performed using a 4D Nucleofector X-Unit (Lonza, CA, USA) according to the manufacturer's instructions as we previously described [13]. ASM cDNA plasmid (pcDNA3.1/V5-His mASM) encoding a full-length *Smpd1* gene under a cytomegalovirus (CMV) immediate early promoter (a gift from Prof. Dr. Erich Gulbins, Essen, Germany). Briefly, CASMCs were tyrpsinized and centrifuged at 90×*g* for 10 minutes. The cell pelletet was resuspended in 100 L P1 Nucleofection solution (Lonza) for Nucleofection (with the program code CM137). The program was chosen based on the fact that Nucleofection efficiency was over 80% as analyzed by flow cytometry using control GFP plasmids. For each Nucleofection sample, 2 μg plasmid DNA was added in 100 L P1 Nucleofection solution. After Nucleofection, cells were cultured in DMEM medium for 24 hours and then cells were ready for the treatments.

Statistics analysis

Data are presented as means ± standard deviation. Significant differences between and within multiple groups were examined using one-way ANOVA test followed by Duncan's multiple-range test. A Students *t* test was used to detect significant difference between two groups. The statistical analysis was performed by SigmaStat 3.5 software (Systat Software, IL). $P<0.05$ was considered statistically significant.

RESULTS

ASM deficiency impaired autophagy in coronary arterial media

The hallmark of autophagy is the formation of the autophagosomes (APs), followed by its fusion with a lysosome leading to maturation of APs into APLs. Microtubule-associated protein 1 light chain (LC3) exists in the cytoplasm in a soluble form (LC3A). A phosphatidylethanolamine (PE)-conjugated form of LC3 (LC3B) is associated with the phagophore and the inner autophagosomal membrane and is a highly specific marker for these structures . Upon fusion with the lysosome, LC3B on the inner autophagosomal membrane is degraded. To examine the significance of ASM in the regulation of autophagic flux *in vivo*, we tested the expression of LC3B as a marker for the accumulation of APs and p62/ubiquitin as markers for autophagic flux in coronary arterial media. As shown in **Fig.1A** and **1C**, representative confocal microscopic images and summarized colocalization coefficient demonstrate that LC3B increased much more in coronary arterial media of ASM-deficient (*Smpd1*$^{-/-}$) mice compared to wild-type (*Smpd1*$^{+/+}$) mice, which colocalized mainly with smooth muscle marker α-smooth muscle actin (α-SMA). As shown in some of yellow areas, colocalization of α-SMA with LC3B was also seen in the intimal area, which might be due to smooth muscle cell migration and infiltration there. In addition, increased ubiquitin and p62 inclusion was detected in the arterial wall of *Smpd1*$^{-/-}$ mice on the Western diet as shown by green and yellow areas in **Fig.1B** and summarized colocalization coefficient in **Fig.1C**, indicating the breakdown of APs in the coronary arterial wall is insufficient. Together, these results demonstrate that the Western diet may stimulate the

formation of APs *in vivo* in coronary arterial media, and the lack of ASM activity results in accumulation of APs and impairment of autophagic flux.

Increased protein expression of LC3B and p62 in ASM-deficient CASMCs

The accumulation of APs and the impairment of autophagic flux was further examined in *Smpd1*$^{-/-}$ CASMCs, which lack ASM activity, using Western blot analysis of LC3B and p62 expression. 7-ketocholesterol is a prototype atherogenic stimulus abundant in oxidized low-density lipoprotein and enhances the expression of LC3B and autophagy in vascular smooth muscle cells [31]. Rapamycin, a classic autophagy stimulus, induces APs formation in a wide variety of cell types and species by inhibiting the activity of mTOR complex 1 (mTORC1) and also regulates APs fusion with lysosomes and autophagic flux [32-33]. As shown in **Fig. 2A** and **2B**, both 7-ketocholesterol and rapamycin-stimulated LC3B expression was significantly enhanced in *Smpd1*$^{-/-}$ CASMCs compared to that in *Smpd1*$^{+/+}$ CASMCs. These results suggest that more APs were formed, or accumulated, in *Smpd1*$^{-/-}$ CASMCs. The abundance of p62, a selective substrate of autophagy degrading pathway, was also higher in *Smpd1*$^{-/-}$ CASMCs, thus, suggesting less p62 protein was degraded due to impaired autophagic flux by knocking out *Smpd1* gene.

ASM is required for the formation of autophagolysosomes (APLs) in CASMCs

Next, we used flow cytometry to analyze the formation of APLs with a lysomotrophic dye, acridine orange, which accumulates in lysosomes with red fluorescence and shows green fluorescence in neutral environment. Since APLs accumulate more acridine orange than normal lysosomes, the red-to-green fluorescent ratio indirectly indicates the change of in the formation of APLs [28]. **Fig.3A** shows *Smpd1*$^{+/+}$ CASMCs treated by either 7-ketocholesterol or rapamycin shifted up to the area with high red fluorescence intensity, which was abolished in *Smpd1*$^{-/-}$ cells. Quantification of the data in **Fig.3B** indicated that ASM deficiency significantly inhibited 7-ketocholesterol or RPM-induced APLs formation in CASMCs. In addition, 7-ketocholesterol or rapamycin-induced APLs formation was also blocked in *Smpd1*$^{+/+}$ cells when ASM activity inhibitor amitriptyline (Ami) was administrated (**Fig.3C**).

Then, we examined whether reduced APLs formation leads to accumulation of APs in CASMCs. To do so, we analyzed the dynamic balance between AP formation and autophagic flux by using a novel dye, CytoID, that exhibits a bright green fluorescence when selectively labeling autophagic vacuoles (APs and APLs). Hypothetically, impaired autophagic flux will result in an increased number of autophagic vacuoles and, consequently, enhancement of the CytoID fluorescence. As shown in **Fig.4A** and **4B**, both 7-ketocholesterol and rapamycin stimulation strongly increased the number of autophagic vacuoles (as shown by increased CytoID-positive cells) in *Smpd1*$^{+/+}$ CASMCs. Such increases in autophagic vacuoles were further enhanced in *Smpd1*$^{-/-}$ CASMCs. We also noticed that even under control condition, more autophagic vacuoles was found in *Smpd1*$^{-/-}$ CASMCs compared to that in *Smpd1*$^{+/+}$ cells (**Fig. 4A** and **Fig.4B)**, indicating that ASM activity may be required for autophagic flux even at resting conditions. When autophagic flux was blocked by chloroquine, a lysosome inhibitor, 7-ketocholesterol or rapamycin

induced similar accumulation of autophagic vacuoles in *Smpd1*$^{+/+}$ CASMCs compared to that in *Smpd1*$^{-/-}$ CASMCs excluding a role of ASM in APs formation (**Fig.4C)**.

ASM deficiency prevents lysosome fusion in CASMCs

To address the possible mechanism mediating the role of ASM in the control of autophagic flux, we examined its role in lysosome fusion to APs - a crucial step during autophagy maturation leading to the formation of APLs. We detected colocalization and fluorescent resonance energy transfer (FRET) between Alexa488-Lamp1 (Lamp1 is a lysosome membrane marker protein) and Alexa555-LC3B (LC3B is an AP marker) in CASMCs. As shown in **Fig. 5A,** both 7-ketocholesterol and rapamycin significantly increased yellow puncta, or patches, in *Smpd1*$^{+/+}$ CASMCs (merged images), indicating increased colocalization of the lysosome marker and AP marker, which may be due to a fusion of both vesicles. However, both 7-ketocholesterol and rapamycin-induced colocalization was markedly reduced in *Smpd1*$^{-/-}$ CASMCs lacking ASM activity compared to *Smpd1*$^{+/+}$ CASMCs. FRET analysis further confirmed this difference in colocalization of lysosomal and autophagosome marker molecules between *Smpd1*$^{-/-}$ and *Smpd1*$^{+/+}$ CASMCs, as shown in blue fluorescent images. Summarized FRET efficiency further confirmed that the FRET between Alexa488-Lamp1 and Alexa555-LC3B was much lower in CASMCs from *Smpd1*$^{-/-}$ than *Smpd1*$^{+/+}$ mice (**Fig. 5B**). Moreover, similar Lamp1-positive puncta were found inbetween *Smpd1*$^{-/-}$ and *Smpd1*$^{+/+}$ CASMCs, which indicates that the decreased colocalization or FRET between Lamp1 and LC3B is not due to either lysosome degeneration or decreased lysosome biogenesis (**Fig. 5C**).

Effects of ASM deficiency on lysosomal cathepsin activities

It has been shown that decreased lysosomal proteolytic activity may inhibit AP turnover resulting in impaired autophagic flux[34]. Thus, we examined whether the role of ASM in autophagic flux is associated with decreased activity of lysosomal proteases such as cathepsin B and cathepsin D. As shown in **Fig. 6A** and **6B**, no difference in cathepsin B or cathepsin D activity was found between *Smpd1*$^{+/+}$ and *Smpd1*$^{-/-}$ CASMCs.

ASM deficiency enhances cell dedifferentiation and proliferation in CASMCs

Next, we examined whether CASMCs lacking ASM activity exibit phenotypic changes to a more proliferative status. In smooth muscle cells, 7-ketocholesterol induced migration and proliferation at a low concentration (<5 μM) [35] but caused apoptosis at higher concentration (100 μM) [36]. As shown in **Fig.7A-C**, 7-ketocholesterol, in a low-concentration range (10 μM), markedly increased expression of dedifferentiation marker vimentin and cell proliferation in *Smpd1*$^{+/+}$ CASMCs. Such 7-ketocholesterol-induced vimentin expression and proliferation was further augmented in *Smpd1*$^{-/-}$ CASMCs lacking ASM activity.

ASM overexpression increases APLs formation under atherogenic stimulation

Furthermore, we investigated whether increased ASM expression is correlated with enhanced APLs formation in CASMCs under atherogenic stimulation. We first determined the effects of 7-ketocholesterol on ASM activity in *Smpd1*$^{+/+}$ CASMCs. We found that 7-

ketocholesterol treatment (0.5-24 h) significantly inhibited ASM activity in *Smpd1*$^{+/+}$ CASMCs by approximately 50% (**Fig. 8A**). This result suggests that increased ASM expression or activity may further enhance 7-ketocholesterol-induced APLs formation in *Smpd1*$^{+/+}$ CASMCs. To test this hypothesis, we transfected *Smpd1*$^{+/+}$ CASMCs with ASM cDNA plasmids by Nucleofection technology, which efficiently caused a 3-fold increase in ASM activity compared to scramble transfection (**Fig.8B**). Interestingly, such ASM overexpression further increased APLs formation in *Smpd1*$^{+/+}$ CASMCs under 7-ketocholesterol stimulation (**Fig.8C**). Moreover, in *Smpd1*$^{-/-}$ CASMCs, ASM overexpression restored the ASM activity and APLs formation under 7-ketocholesterol stimulation to a similar level to those in *Smpd1*$^{+/+}$ CASMCs. Thus, these data strongly suggest that ASM expression is correlated with APLs formation under 7-ketocholesterol stimulation (**Fig.8B** and **8C**).

DISCUSSION

The goal of the present study is to determine whether ASM plays a protective role in coronary atherosclerosis by controlling autophagic flux in CASMCs and their phenotypic status. ASM deficiency results in a defective form of autophagic flux in the coronary arterial media of mice fed a Western diet or in primary cultured CASMCs under atherogenic stimulation. This defective form of autophagic flux was attributed to the lack of lysosomes fusion with APs and consequent impaired autophagy maturation. Our results demonstrate that ASM plays a permissive role in targeting lysosomes to APs leading to autophagy maturation and effective autophagic flux, which protects SMCs from cell dedifferentiation to proliferative phenotypes.

Our findings demonstrate an important role of ASM, a critical enzyme involved in the sphingolipid metabolism, in controlling autophagic flux. LC3B specifically associates with AP membranes and is degraded on the inner APL membrane upon fusion with the lysosome [17, 37]. P62 binds directly to LC3B to trigger autophagic degradation of p62-positive cytoplasmic inclusion bodies [38]. Therefore, the simultaneous increase in LC3B and p62 protein expression suggests a failed breakdown of APs due to impaired autophagic flux. Here, we demonstrated that a deficiency of ASM results in an impaired autophagic flux in coronary arterial media of mice fed a high fat Western diet and in CASMCs under atherogenic stimulation as characterized by increased expression of LC3B and p62. Consistently, our flow cytometric analysis showed that ASM deficiency resulted in decreased formation of APLs and enhanced accumulation of APs under atherogenic stimulation. A few recent studies reported that ASM is involved in the autophagy induction in cancer cells [39-40]. ASM is requried for upregulation of Atg5 expression resulting in autophagy induction in HEPG2 hepatoma cells [39]. Knockdown of ASM significantly suppressed the autophagy induction in leukemia HL-60 cells under amino acid deprivation [40]. In the present study, however, when the autophagic flux was blocked, 7-ketocholesterol-induced APs accumulation was similar in ASM-deficient CASMCs compared to wild-type cells, which rules out the role of ASM in APs formation. This discrepency regarding the role of ASM in early or late phase of autophagy is unclear, which may be due to the differences in the types of cells and stimuli used.

Our data further demonstrated a lack of APs fusion with lysosomes in ASM-deficient CASMCs indicating a role of ASM in autophagy maturation by controlling lysosomes trafficking and fusion with APs. ASM is the key enzyme to hydrolyze sphingomyelin to ceramide in lysosomes and its deficiency commonly causes altered 'sphingolipid rheostat' with abnormal levels of sphingolipid species including sphingomyelin, ceramide, sphingosine and their phosphorylated metabolites [40], which can be major regulators for Ca^{2+}-dependent lysosomal trafficking function [41-43]. Lysosomal accumulation of sphingomyelin by ASM deficiency has recently been shown to inhibit the activity of a principle lysosomal Ca^{2+} channel, mucolipin transient receptor potential channel 1 (TRPML1), and thereby block the lysosomal Ca^{2+}-dependent membrane trafficking [43]. A target protein regulated by lysosomal Ca^{2+} is dynein, a multi-subunit microtubule motor protein complex, which is responsible for nearly all minus-end microtubule-based transport of vesicles within eukaryotic cells and is recently implicated in lysosome and AP trafficking to meet and form APLs [33, 44]. Inhibition or loss of dynein function abolishes lysosome fusion with APs and increases the number of APs in glioma, or neuronal cells, and in CASMCs [44-45]. These previous studies suggest that ASM-regulated lysosomal trafficking function may be associated with the level of lysosomal sphingomyelin via regulating TRPML1/lysosomal Ca^{2+}/dynein signaling axis in CASMCs. In another aspect, ceramide, an ASM product, is a highly hydrophobic lipid that has been shown to participate in lysosome fusion to the cell plasma membrane, endosomes, phagosomes and other organelles [30, 46-47]. Ceramide also regulates cytoskeleton and microtubule assembly, which plays a crucial role in vesicular trafficking in mammalian cells [48-50]. Ceramide can directly interact with LC3B that may facilitate the targeting of lysosomes to APs [51]. In constrast, overproduction of ceramide or its metabolite sphingosine may increase lysosome permeability leading to impaired autophagy maturation [52]. Therefore, in addition to sphingomyelin, lysosomal ASM-derived ceramide and subsequent metabolites may also actively control autophagy maturation. Collectively, our data and previous observations support the view that lysosomal trafficiking function in CASMCs is associated with their lysosomal sphingolipid profile rather than one specific sphingolipid.

Previous studies have demonstrated a functional relationship between ASM and lysosomal cathepsin B and that ASM deficiency leads to the enhanced processing and activation of cathepsin B in hepatic stellate cells [53]. Further, the decreased lysosomal proteolytic activity of cathepsins inhibits APs turnover leading to impaired autophagic flux but does not affect the AP-lysosome fusion event [34]. However, our data from *in vitro* cathepsin substrate assay showed that ASM deficiency did not alter lysosomal protease activity such as cathepsins B and D activity in CASMCs. The discrepancy regarding the role of ASM in cathepsins acitivity between CASMCs and hepatic stellate cells is unknown. It is possible that modulation of lysosomal cathepsin activity in CASMCs is either ASM-independent or compensated by other signaling pathways. Nontheless, our data support the view that a defective autophagic flux in ASM-deficient CASMCs is primarily due to impaired autophagy maturation with deregulated lysosomal function to traffic and fuse with APs.

In the vasculature of progressive atherosclerosis or restenosis after coronary angioplasty, moderately enhanced autophagy is protective by preventing an imbalance of vascular SMCs homeostasis, which helps vascular smooth muscle in differentiated contractile phenotype,

and thereby decreases cell proliferation and prevents fibrosis [11]. Autophagy has anti-proliferative effects on smooth muscle cells under various atherogenic stimuli such as thrombin and advanced glycation end products [54-55]. We previously showed that enhanced autophagy by either statins or rapamycin is an important mechanism for maintaining a contractile phenotype in CASMCs and inhibiting their proliferation during atherogenic stimulation [13]. The present study showed that 7-ketocholesterol increased vimentin expression (a dedifferentiation marker) and proliferation in wild-type CASMCs, which were augmented in ASM-deficient CASMCs. Together, these data implicate that the role of ASM in autophagy maturation is protective in atherosclerosis by modulating smooth muscle cell phenotypic properties.

Our findings that 7-ketocholesterol partially inhibited ASM activity is consistent with previous studies that showed similar inhibition of ASM activity by 7-ketocholesterol or oxidized low-density lipoprotein in a cell-free system [56]. Additionally, forced expression of ASM further enhanced 7-ketocholesterol-induced APLs formation in wild-type CASMCs and completely restored APLs formation in ASM-deficient CASMCs. These data indicate that ASM overexpression may enhance autophagy maturation in wild-type CASMCs with compromised ASM activity, such as those under atherogenic stimulation, or restore the potential of ASM-deficient CASMCs for effecient autophagy maturation. Such correlation between ASM expression and autophagy maturation further confirms a crucial role of ASM in facilitating autophagic flux in smooth muscle cells under atherogenic stimulation. Overexpression of ASM ameliorates aortic lesions in mouse models of atherosclerosis [2]; however, its exact roles in treating atherosclerosis are unknown. It has been proposed that overexpressed ASM proteins exert their protective effects by acting locally on resident macrophages in the arterial wall and/or altering circulating lipoproteins [2]. Here, our findings provide new insights for the protective role of ASM overexpression in atherosclerosis, which is associated with improved lysosome trafficking function and consequent autophagy maturation in smooth muscle cells.

In summary, the present study reveals that in CASMCs, ASM controls autophagy maturation by regulating lysosome trafficking and fusion to APs and consequent autophagic flux. Defects in this lysosomal regulation of autophagy in CASMCs may result in defective autophagic flux characterized by the accumulation of APs, the reduction in APLs formation and impaired autophagic flux, which may result in imbalance of arterial smooth muscle homeostasis and ultimately induces, or accelerates, coronary atherosclerosis during hyperlipidemia or hypercholesteremia. Our data implicate a protective role of ASM in atherosclerosis via its tonic regulation of autophagy maturation in arterial smooth muscle cells. Clinically, recombinant human ASM has been used for Niemman-Pick patients and patients with cancer [57-58]. Therefore, our study provides further evidence that such recombinant human ASM therapy may be used to treat atherosclerosis in humans.

Acknowledgments

This study was supported by grants from the National Institutes of Health (HL-57244, HL-075316, and HL-091464), National Institute of Health CTSA grant UL1TR000058 and VCU CCTR Endowment Fund.

Reference

1. Zhang Y, Li X, Becker KA, Gulbins E. Ceramide-enriched membrane domains--structure and function. Biochim Biophys Acta. 2009; 1788:178–183. [PubMed: 18786504]
2. Leger AJ, Mosquea LM, Li L, Chuang W, Pacheco J, Taylor K, Luo Z, Piepenhagen P, Ziegler R, Moreland R, Urabe A, Jiang C, Cheng SH, Yew NS. Adeno-associated virus-mediated expression of acid sphingomyelinase decreases atherosclerotic lesion formation in apolipoprotein E(−/−) mice. J Gene Med. 2011; 13:324–332. [PubMed: 21674735]
3. Devlin CM, Leventhal AR, Kuriakose G, Schuchman EH, Williams KJ, Tabas I. Acid sphingomyelinase promotes lipoprotein retention within early atheromata and accelerates lesion progression. Arterioscler Thromb Vasc Biol. 2008; 28:1723–1730. [PubMed: 18669882]
4. Schissel SL, Keesler GA, Schuchman EH, Williams KJ, Tabas I. The cellular trafficking and zinc dependence of secretory and lysosomal sphingomyelinase, two products of the acid sphingomyelinase gene. J Biol Chem. 1998; 273:18250–18259. [PubMed: 9660788]
5. Tabas I, Williams KJ, Boren J. Subendothelial lipoprotein retention as the initiating process in atherosclerosis: update and therapeutic implications. Circulation. 2007; 116:1832–1844. [PubMed: 17938300]
6. Oorni K, Posio P, Ala-Korpela M, Jauhiainen M, Kovanen PT. Sphingomyelinase induces aggregation and fusion of small very low-density lipoprotein and intermediate-density lipoprotein particles and increases their retention to human arterial proteoglycans. Arterioscler Thromb Vasc Biol. 2005; 25:1678–1683. [PubMed: 15879301]
7. Leventhal AR, Chen W, Tall AR, Tabas I. Acid sphingomyelinase-deficient macrophages have defective cholesterol trafficking and efflux. J Biol Chem. 2001; 276:44976–44983. [PubMed: 11579092]
8. Liu J, Huan C, Chakraborty M, Zhang H, Lu D, Kuo MS, Cao G, Jiang XC. Macrophage sphingomyelin synthase 2 deficiency decreases atherosclerosis in mice. Circ Res. 2009; 105:295–303. [PubMed: 19590047]
9. McGovern MM, Pohl-Worgall T, Deckelbaum RJ, Simpson W, Mendelson D, Desnick RJ, Schuchman EH, Wasserstein MP. Lipid abnormalities in children with types A and B Niemann Pick disease. J Pediatr. 2004; 145:77–81. [PubMed: 15238911]
10. Fuster JJ, Fernandez P, Gonzalez-Navarro H, Silvestre C, Nabah YN, Andres V. Control of cell proliferation in atherosclerosis: insights from animal models and human studies. Cardiovasc Res. 2010; 86:254–264. [PubMed: 19900964]
11. Lacolley P, Regnault V, Nicoletti A, Li Z, Michel JB. The vascular smooth muscle cell in arterial pathology: a cell that can take on multiple roles. Cardiovasc Res. 2012; 95:194–204. [PubMed: 22467316]
12. Klionsky DJ, Emr SD. Autophagy as a regulated pathway of cellular degradation. Science. 2000; 290:1717–1721. [PubMed: 11099404]
13. Wei YM, Li X, Xu M, Abais JM, Chen Y, Riebling CR, Boini KM, Li PL, Zhang Y. Enhancement of autophagy by simvastatin through inhibition of Rac1-mTOR signaling pathway in coronary arterial myocytes. Cell Physiol Biochem. 2013; 31:925–937. [PubMed: 23817226]
14. Levine B, Kroemer G. Autophagy in the pathogenesis of disease. Cell. 2008; 132:27–42. [PubMed: 18191218]
15. Klionsky DJ. Autophagy: from phenomenology to molecular understanding in less than a decade. Nat Rev Mol Cell Biol. 2007; 8:931–937. [PubMed: 17712358]
16. Bampton ET, Goemans CG, Niranjan D, Mizushima N, Tolkovsky AM. The dynamics of autophagy visualized in live cells: from autophagosome formation to fusion with endo/lysosomes. Autophagy. 2005; 1:23–36. [PubMed: 16874023]
17. Xie Z, Klionsky DJ. Autophagosome formation: core machinery and adaptations. Nat Cell Biol. 2007; 9:1102–1109. [PubMed: 17909521]
18. Boini KM, Xia M, Li C, Zhang C, Payne LP, Abais JM, Poklis JL, Hylemon PB, Li PL. Acid sphingomyelinase gene deficiency ameliorates the hyperhomocysteinemia-induced glomerular injury in mice. Am J Pathol. 2011; 179:2210–2219. [PubMed: 21893018]

19. Li X, Han WQ, Boini KM, Xia M, Zhang Y, Li PL. TRAIL death receptor 4 signaling via lysosome fusion and membrane raft clustering in coronary arterial endothelial cells: evidence from ASM knockout mice. J Mol Med (Berl). 2013; 91:25–36. [PubMed: 23108456]
20. Lemaitre V, Soloway PD, D'Armiento J. Increased medial degradation with pseudo-aneurysm formation in apolipoprotein E-knockout mice deficient in tissue inhibitor of metalloproteinases-1. Circulation. 2003; 107:333–338. [PubMed: 12538437]
21. Park TS, Panek RL, Mueller SB, Hanselman JC, Rosebury WS, Robertson AW, Kindt EK, Homan R, Karathanasis SK, Rekhter MD. Inhibition of sphingomyelin synthesis reduces atherogenesis in apolipoprotein E-knockout mice. Circulation. 2004; 110:3465–3471. [PubMed: 15545514]
22. Bjursell M, Gerdin AK, Lelliott CJ, Egecioglu E, Elmgren A, Tornell J, Oscarsson J, Bohlooly YM. Acutely reduced locomotor activity is a major contributor to Western diet-induced obesity in mice. Am J Physiol Endocrinol Metab. 2008; 294:E251–260. [PubMed: 18029443]
23. Wei YM, Li X, Xiong J, Abais JM, Xia M, Boini KM, Zhang Y, Li PL. Attenuation by statins of membrane raft-redox signaling in coronary arterial endothelium. J Pharmacol Exp Ther. 2013; 345:170–179. [PubMed: 23435541]
24. Becker KA, Henry B, Ziobro R, Tummler B, Gulbins E, Grassme H. Role of CD95 in pulmonary inflammation and infection in cystic fibrosis. J Mol Med (Berl). 2012; 90:1011–1023. [PubMed: 22314624]
25. Xu M, Zhang Y, Xia M, Li XX, Ritter JK, Zhang F, Li PL. NAD(P)H oxidase-dependent intracellular and extracellular O2*-production in coronary arterial myocytes from CD38 knockout mice. Free Radic Biol Med. 2012; 52:357–365. [PubMed: 22100343]
26. Zhang Y, Li X, Carpinteiro A, Gulbins E. Acid sphingomyelinase amplifies redox signaling in Pseudomonas aeruginosa-induced macrophage apoptosis. J Immunol. 2008; 181:4247–4254. [PubMed: 18768882]
27. Zhang C, Boini KM, Xia M, Abais JM, Li X, Liu Q, Li PL. Activation of Nod-like receptor protein 3 inflammasomes turns on podocyte injury and glomerular sclerosis in hyperhomocysteinemia. Hypertension. 2012; 60:154–162. [PubMed: 22647887]
28. Raben N, Shea L, Hill V, Plotz P. Monitoring autophagy in lysosomal storage disorders. Methods Enzymol. 2009; 453:417–449. [PubMed: 19216919]
29. Zhang Y, Li X, Carpinteiro A, Goettel JA, Soddemann M, Gulbins E. Kinase suppressor of Ras-1 protects against pulmonary Pseudomonas aeruginosa infections. Nat Med. 2011; 17:341–346. [PubMed: 21297617]
30. Jin S, Yi F, Zhang F, Poklis JL, Li PL. Lysosomal targeting and trafficking of acid sphingomyelinase to lipid raft platforms in coronary endothelial cells. Arterioscler Thromb Vasc Biol. 2008; 28:2056–2062. [PubMed: 18772496]
31. Ding Z, Wang X, Schnackenberg L, Khaidakov M, Liu S, Singla S, Dai Y, Mehta JL. Regulation of autophagy and apoptosis in response to ox-LDL in vascular smooth muscle cells, and the modulatory effects of the microRNA hsa-let-7g. Int J Cardiol. 2013; 168:1378–1385. [PubMed: 23305858]
32. Zhou C, Zhong W, Zhou J, Sheng F, Fang Z, Wei Y, Chen Y, Deng X, Xia B, Lin J. Monitoring autophagic flux by an improved tandem fluorescent-tagged LC3 (mTagRFP-mWasabi-LC3) reveals that high-dose rapamycin impairs autophagic flux in cancer cells. Autophagy. 2012; 8:1215–1226. [PubMed: 22647982]
33. Jahreiss L, Menzies FM, Rubinsztein DC. The itinerary of autophagosomes: from peripheral formation to kiss-and-run fusion with lysosomes. Traffic. 2008; 9:574–587. [PubMed: 18182013]
34. Yue W, Hamai A, Tonelli G, Bauvy C, Nicolas V, Tharinger H, Codogno P, Mehrpour M. Inhibition of the autophagic flux by salinomycin in breast cancer stem-like/progenitor cells interferes with their maintenance. Autophagy. 2013; 9:714–729. [PubMed: 23519090]
35. Liao PL, Cheng YW, Li CH, Wang YT, Kang JJ. 7-Ketocholesterol and cholesterol-5alpha,6alpha-epoxide induce smooth muscle cell migration and proliferation through the epidermal growth factor receptor/phosphoinositide 3-kinase/Akt signaling pathways. Toxicol Lett. 2010; 197:88–96. [PubMed: 20466046]
36. Pedruzzi E, Guichard C, Ollivier V, Driss F, Fay M, Prunet C, Marie JC, Pouzet C, Samadi M, Elbim C, O'Dowd Y, Bens M, Vandewalle A, Gougerot-Pocidalo MA, Lizard G, Ogier-Denis E.

NAD(P)H oxidase Nox-4 mediates 7-ketocholesterol-induced endoplasmic reticulum stress and apoptosis in human aortic smooth muscle cells. Mol Cell Biol. 2004; 24:10703–10717. [PubMed: 15572675]

37. Kabeya Y, Mizushima N, Ueno T, Yamamoto A, Kirisako T, Noda T, Kominami E, Ohsumi Y, Yoshimori T. LC3, a mammalian homologue of yeast Apg8p, is localized in autophagosome membranes after processing. EMBO J. 2000; 19:5720–5728. [PubMed: 11060023]
38. Pankiv S, Clausen TH, Lamark T, Brech A, Bruun JA, Outzen H, Overvatn A, Bjorkoy G, Johansen T. p62/SQSTM1 binds directly to Atg8/LC3 to facilitate degradation of ubiquitinated protein aggregates by autophagy. J Biol Chem. 2007; 282:24131–24145. [PubMed: 17580304]
39. Park MA, Zhang G, Martin AP, Hamed H, Mitchell C, Hylemon PB, Graf M, Rahmani M, Ryan K, Liu X, Spiegel S, Norris J, Fisher PB, Grant S, Dent P. Vorinostat and sorafenib increase ER stress, autophagy and apoptosis via ceramide-dependent CD95 and PERK activation. Cancer Biol Ther. 2008; 7:1648–1662. [PubMed: 18787411]
40. Taniguchi M, Kitatani K, Kondo T, Hashimoto-Nishimura M, Asano S, Hayashi A, Mitsutake S, Igarashi Y, Umehara H, Takeya H, Kigawa J, Okazaki T. Regulation of autophagy and its associated cell death by “sphingolipid rheostat”: reciprocal role of ceramide and sphingosine 1-phosphate in the mammalian target of rapamycin pathway. J Biol Chem. 2012; 287:39898–39910. [PubMed: 23035115]
41. Glunde K, Guggino SE, Solaiyappan M, Pathak AP, Ichikawa Y, Bhujwalla ZM. Extracellular acidification alters lysosomal trafficking in human breast cancer cells. Neoplasia. 2003; 5:533–545. [PubMed: 14965446]
42. Trajkovic K, Dhaunchak AS, Goncalves JT, Wenzel D, Schneider A, Bunt G, Nave KA, Simons M. Neuron to glia signaling triggers myelin membrane exocytosis from endosomal storage sites. J Cell Biol. 2006; 172:937–948. [PubMed: 16520383]
43. Shen D, Wang X, Li X, Zhang X, Yao Z, Dibble S, Dong XP, Yu T, Lieberman AP, Showalter HD, Xu H. Lipid storage disorders block lysosomal trafficking by inhibiting a TRP channel and lysosomal calcium release. Nat Commun. 2012; 3:731. [PubMed: 22415822]
44. Yamamoto M, Suzuki SO, Himeno M. The effects of dynein inhibition on the autophagic pathway in glioma cells. Neuropathology. 2010; 30:1–6. [PubMed: 19496938]
45. Xu M, Li XX, Xiong J, Xia M, Gulbins E, Zhang Y, Li PL. Regulation of autophagic flux by dynein-mediated autophagosomes trafficking in mouse coronary arterial myocytes. Biochim Biophys Acta. 2013; 1833:3228–3236. [PubMed: 24095928]
46. Schramm M, Herz J, Haas A, Kronke M, Utermohlen O. Acid sphingomyelinase is required for efficient phago-lysosomal fusion. Cell Microbiol. 2008; 10:1839–1853. [PubMed: 18485117]
47. Trajkovic K, Hsu C, Chiantia S, Rajendran L, Wenzel D, Wieland F, Schwille P, Brugger B, Simons M. Ceramide triggers budding of exosome vesicles into multivesicular endosomes. Science. 2008; 319:1244–1247. [PubMed: 18309083]
48. Zeidan YH, Jenkins RW, Hannun YA. Remodeling of cellular cytoskeleton by the acid 22 sphingomyelinase/ceramide pathway. J Cell Biol. 2008; 181:335–350. [PubMed: 18426979]
49. Lee YG, Lee J, Cho JY. Cell-permeable ceramides act as novel regulators of U937 cell-cell adhesion mediated by CD29, CD98, and CD147. Immunobiology. 2010; 215:294–303. [PubMed: 19576658]
50. Widau RC, Jin Y, Dixon SA, Wadzinski BE, Gallagher PJ. Protein phosphatase 2A (PP2A) holoenzymes regulate death-associated protein kinase (DAPK) in ceramide-induced anoikis. J Biol Chem. 2010; 285:13827–13838. [PubMed: 20220139]
51. Sentelle RD, Senkal CE, Jiang W, Ponnusamy S, Gencer S, Selvam SP, Ramshesh VK, Peterson YK, Lemasters JJ, Szulc ZM, Bielawski J, Ogretmen B. Ceramide targets autophagosomes to mitochondria and induces lethal mitophagy. Nat Chem Biol. 2012; 8:831–838. [PubMed: 22922758]
52. Patschan S, Chen J, Polotskaia A, Mendelev N, Cheng J, Patschan D, Goligorsky MS. Lipid mediators of autophagy in stress-induced premature senescence of endothelial cells. Am J Physiol Heart Circ Physiol. 2008; 294:H1119–1129. [PubMed: 18203850]

53. Moles A, Tarrats N, Fernandez-Checa JC, Mari M. Cathepsin B overexpression due to acid sphingomyelinase ablation promotes liver fibrosis in Niemann-Pick disease. J Biol Chem. 2012; 287:1178–1188. [PubMed: 22102288]

54. Dong N, Zhu Q, Zhang P, Zhu C, Wang M, Li W, Liu J, Liu Y, Ma B, Wu K. Autophagy downregulates thrombin-induced VSMCs proliferation through lysosomal pathway. Int J Cardiol. 2012; 159:156–158. [PubMed: 22704878]

55. Hu P, Lai D, Lu P, Gao J, He H. ERK and Akt signaling pathways are involved in advanced glycation end product-induced autophagy in rat vascular smooth muscle cells. Int J Mol Med. 2012; 29:613–618. [PubMed: 22293957]

56. Maor I, Mandel H, Aviram M. Macrophage uptake of oxidized LDL inhibits lysosomal sphingomyelinase, thus causing the accumulation of unesterified cholesterol-sphingomyelin-rich particles in the lysosomes. A possible role for 7-Ketocholesterol. Arterioscler Thromb Vasc Biol. 1995; 15:1378–1387. [PubMed: 7670952]

57. Thurberg BL, Wasserstein MP, Schiano T, O'Brien F, Richards S, Cox GF, McGovern MM. Liver and skin histopathology in adults with acid sphingomyelinase deficiency (Niemann-Pick disease type B). Am J Surg Pathol. 2012; 36:1234–1246. [PubMed: 22613999]

58. Savic R, He X, Fiel I, Schuchman EH. Recombinant human acid sphingomyelinase as an adjuvant to sorafenib treatment of experimental liver cancer. PLoS One. 2013; 8:e65620. [PubMed: 23724146]

Key messages

Acid sphingomyelinase (ASM) controls autophagy maturation in smooth muscle cells

ASM maintains smooth muscle cell homeostasis and its contractile phenotype

ASM plays a protective role in smooth muscle dysfunction and atherosclerosis

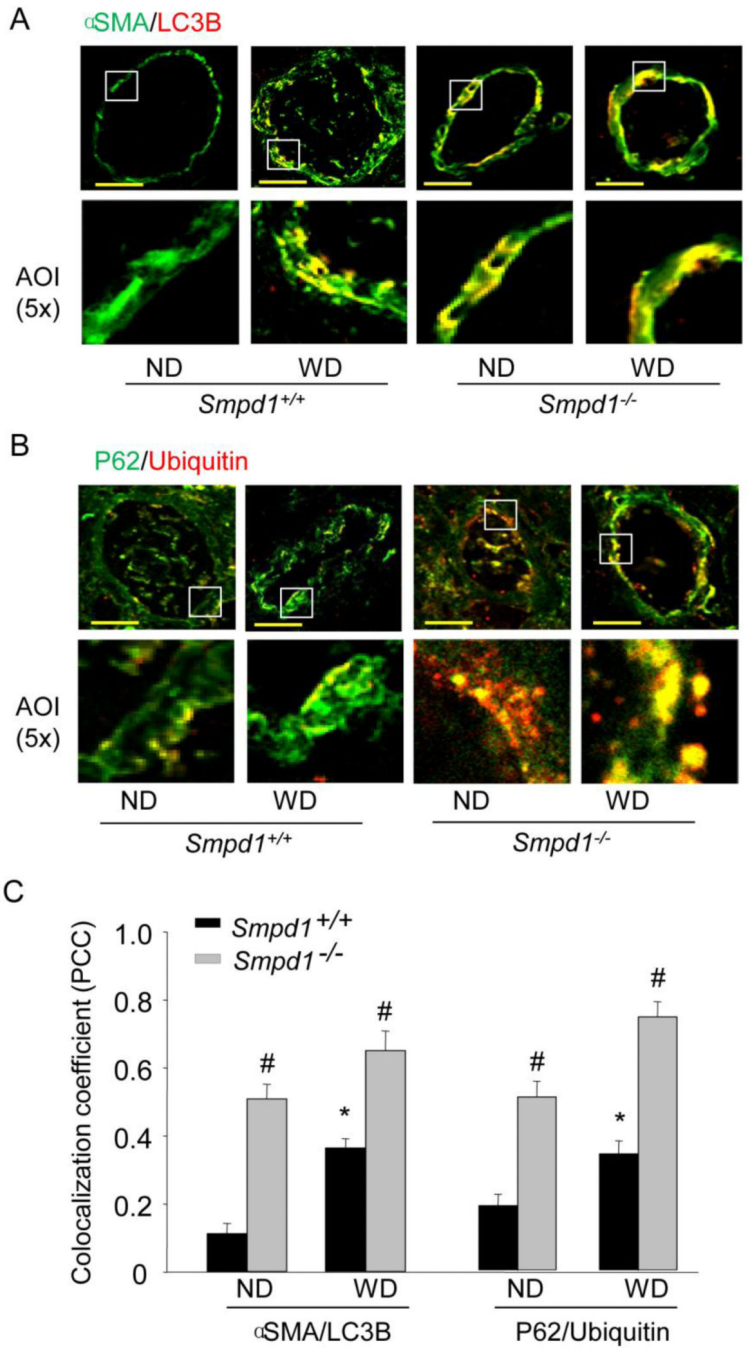

Figure 1. Deregulated autophagic process in coronary arterial media of ASM-deficient mice fed Western diet

Wild-type (*Smpd1*$^{+/+}$) and ASM-deficient (*Smpd1*$^{-/-}$) mice were fed either a normal diet (ND) or a high fat Western diet (WD) for 10 weeks. Coronary arteries of mouse hearts were dissected and used for confocal immunofluorescent analysis. (A) Representative confocal fluorescence images of autophagy marker LC3B with smooth muscle marker α-SMA in coronary arteries of mice fed ND or WD. Scale bar: 50 μm. (B) Representative confocal fluorescence images of ubiquitin with p62 in coronary arteries of mice fed ND or WD. (C) Summarized colocalization coefficient (PCC) of LC3B with α-SMA or ubiquintin with p62

in coronary arteries of mice fed ND or WD. *P<0.05 *vs.* $Smpd1^{+/+}$ ND; #$P < 0.05$ $Smpd1^{-/-}$ *vs.* $Smpd1^{+/+}$ (n=6).

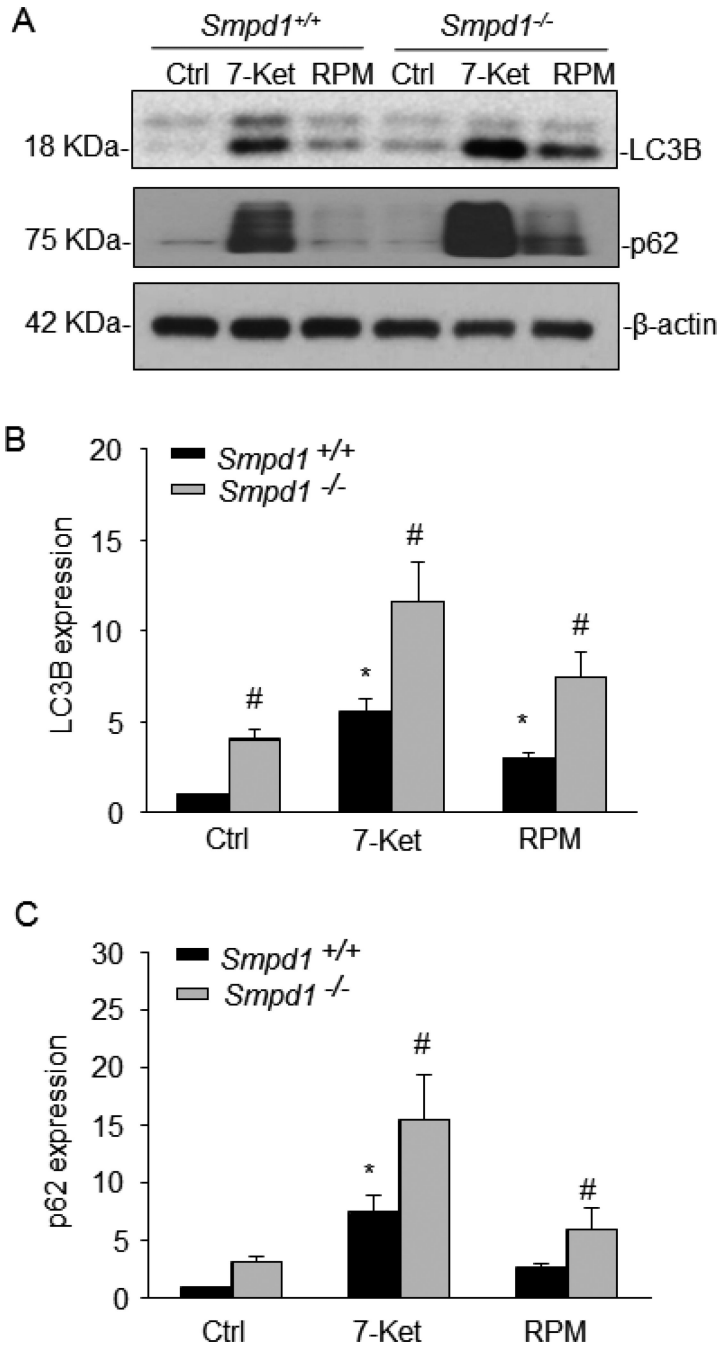

Figure 2. ASM deficiency increases the expression of LC3B and p62 upon atherogenic stimulation

Mouse CASMCs were under control condition or stimulated with 7-ketocholesterol (7-Ket, 10 μM) or rapamycin (RPM, 20 nM) for 24 hours. (A) Representative Western blot gel documents showing the protein expression of LC3B, p62 and β-actin in *Smpd1*$^{+/+}$ or *Smpd1*$^{-/-}$ CASMCs. (B) and (C) are summarized data. *P<0.05 *vs. Smpd1*$^{+/+}$ control; #*P* < 0.05 *Smpd1*$^{-/-}$ *vs. Smpd1*$^{+/+}$ (n=6).

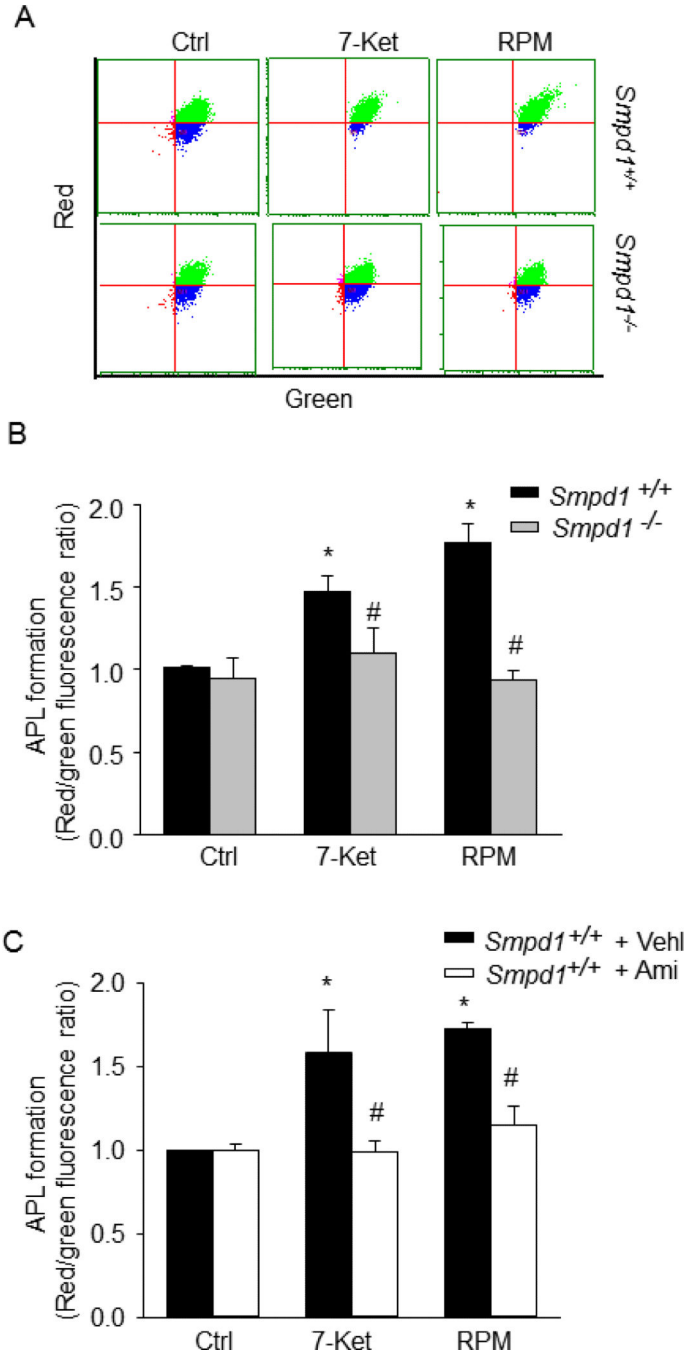

Figure 3. Decreased formation of autophagolysosomes (APLs) in ASM-deficient CASMCs upon atherogenic stimulation

Mouse CASMCs were under control condition or stimulated with 7-ketocholesterol (7-Ket, 10 μM) or rapamycin (RPM, 20 nM) for 24 hours. Mouse CASMCs were then stained with acridine orange (2 g/mL) for 17 min. (A) and (B) Representative dot plots of flow cytometry analysis and summarized red-to-green fluorescence ratio of acridine orange staining showing the formation of APLs in *Smpd1*$^{+/+}$ and *Smpd1*$^{-/-}$ CASMCs. *P<0.05 *vs.* *Smpd1*$^{+/+}$ control; #*P* < 0.05 *Smpd1*$^{-/-}$ *vs. Smpd1*$^{+/+}$ (n=6). (C) Summarized red-to-green fluorescence ratio of acridine orange staining in *Smpd1*$^{+/+}$ CASMCs treated with vehicle

PBS (Vehl) or ASM inhibitor amitriptyline (Ami, 10 μM). *P<0.05 *vs.* *Smpd1*$^{+/+}$ control; #*P* < 0.05 Ami *vs.* Vehl (n=6).

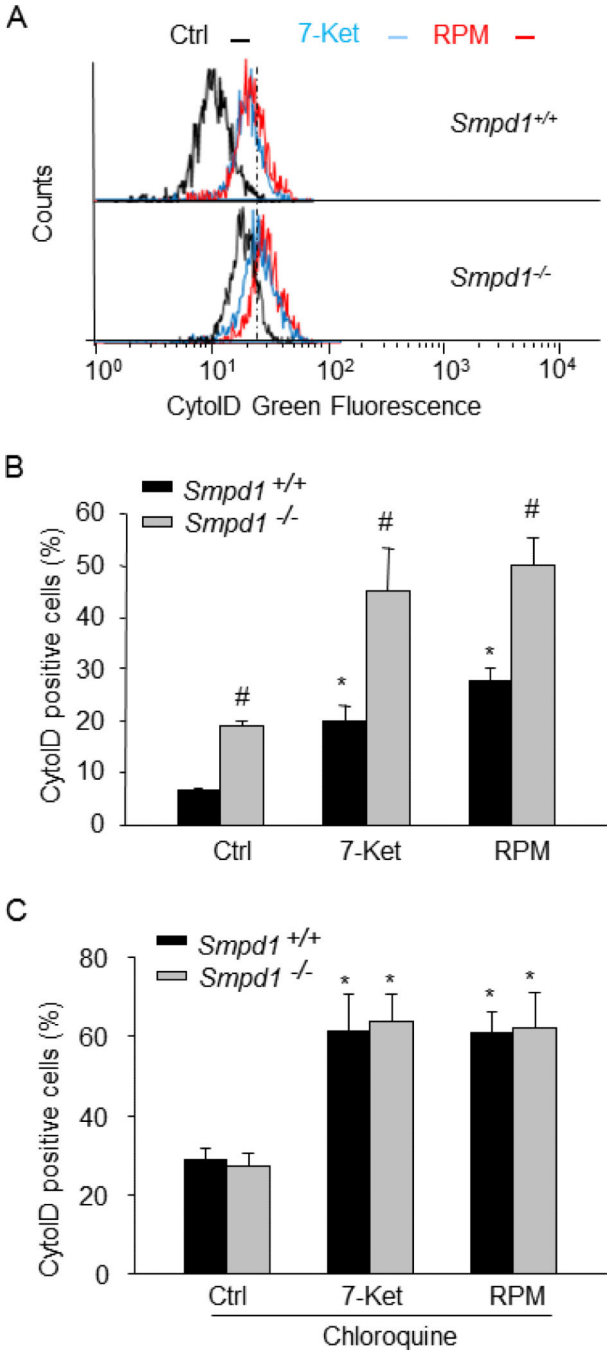

Figure 4. ASM deficiency increases the accumulation of autophagosomes (APs) in CASMCs

Mouse CASMCs were under control condition or stimulated with 7-ketocholesterol (7-Ket, 10 μM) or rapamycin (RPM, 20 nM) for 24 hours in the absence or presence of chloroquine (100 μM). Mouse CASMCs were then stained with CytoID fluorescent probes that detect intracellular autophagosomes. (A) Shown are the representative histograms for flow cytometric analysis of CytoID Green fluorescence in *Smpd1*$^{+/+}$ or *Smpd1*$^{-/-}$ CASMCs treated with control, 7-Ket or RPM. (B) Summarized data showing the percentage of cells that were positive for CytoID Green fluorescence in *Smpd1*$^{+/+}$ or *Smpd1*$^{-/-}$ CASMCs. (C)

Summarized data show the effect of autophagic flux inhibitor chloroquine on the percentage of CytoID-positive cells in *Smpd1*$^{+/+}$ or *Smpd1*$^{-/-}$ CASMCs. *P<0.05 *vs. Smpd1*$^{+/+}$ control; #*P* < 0.05 *Smpd1*$^{-/-}$ *vs. Smpd1*$^{+/+}$ (n=6).

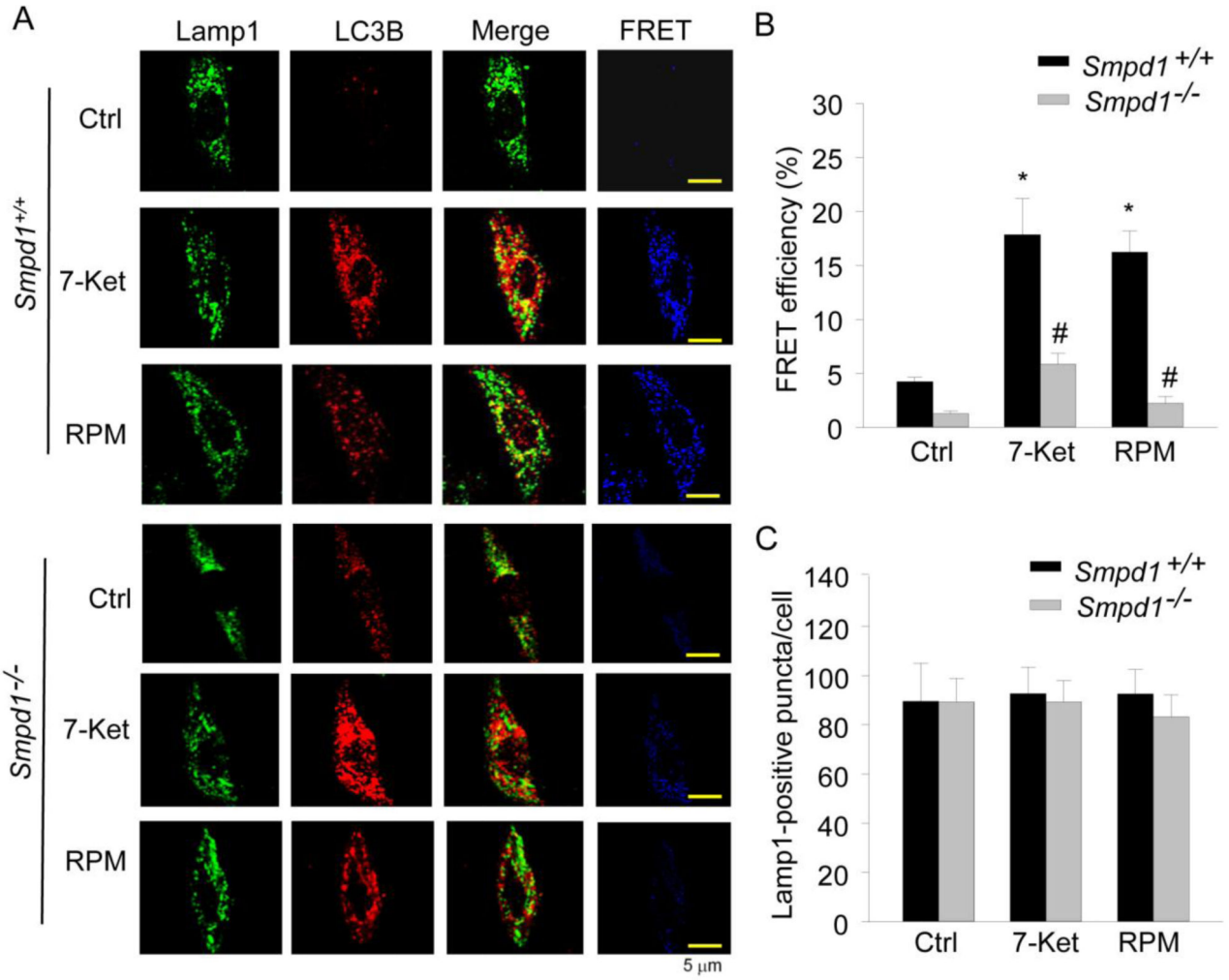

Figure 5. Lacking of autophagosome (AP) fusion with lysosome in ASM-deficient CASMCs

Mouse CASMCs cultured in coverslips were under control condition or stimulated with 7-ketocholesterol (7-Ket, 10 μM) or rapamycin (RPM, 20 nM) for 24 hours. Mouse CASMCs were then fixed, permeabilized and stained with fluorescence-labelled antibodies against LC3B and Lamp1. (A) Representative confocal images of fluorescence resonance energy transfer (FRET) between Alexa488-Lamp-1 and Alexa555-LC3B in *Smpd1*$^{+/+}$ or *Smpd1*$^{-/-}$ CASMCs. The FRET images were obtained by subtraction of the pre-bleaching images from the post-bleaching images and shown in dark blue color. Increased intensity of blue color represents higher level of FRET in these cells. (B) Summarized data show the effect of 7-Ket or RPM on FRET efficiency between Alexa488-Lamp-1 and Alexa555-LC3B in *Smpd1*$^{+/+}$ and *Smpd1*$^{-/-}$ CASMCs (n=4). (C) Summarized data show the effect of 7-Ket or RPM on lysosome biogenesis as quantified by Lamp1-positive vesicles per cell. *P<0.05 *vs.* *Smpd1*$^{+/+}$ control; #*P* < 0.05 *Smpd1*$^{-/-}$ *vs. Smpd1*$^{+/+}$ (n=6).

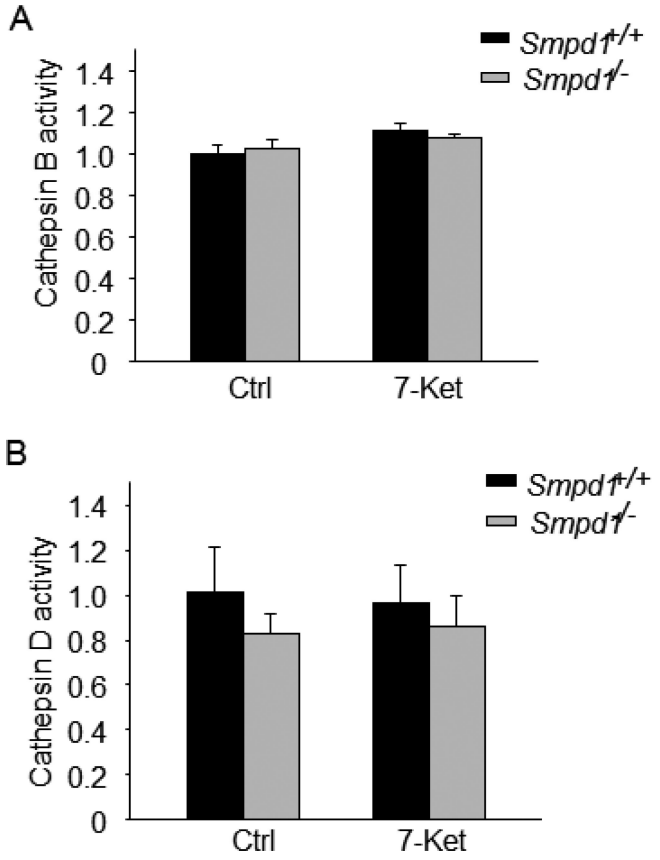

Figure 6. ASM activity and lysosomal cathepsin activity in CASMCs upon atherogenic stimulation

(A) and (B) Summarized data show the catalytic activities for lysosomal cathepsin B and D by fluorogenic substrate assay in *Smpd1*$^{+/+}$ and *Smpd1*$^{-/-}$ CASMCs under control or 7-Ket (10 μM; 24 hours) stimulation. * P<0.05 *vs. Smpd1*$^{+/+}$ control; #*P* < 0.05 *Smpd1*$^{-/-}$ *vs. Smpd1*$^{+/+}$ (n=4).

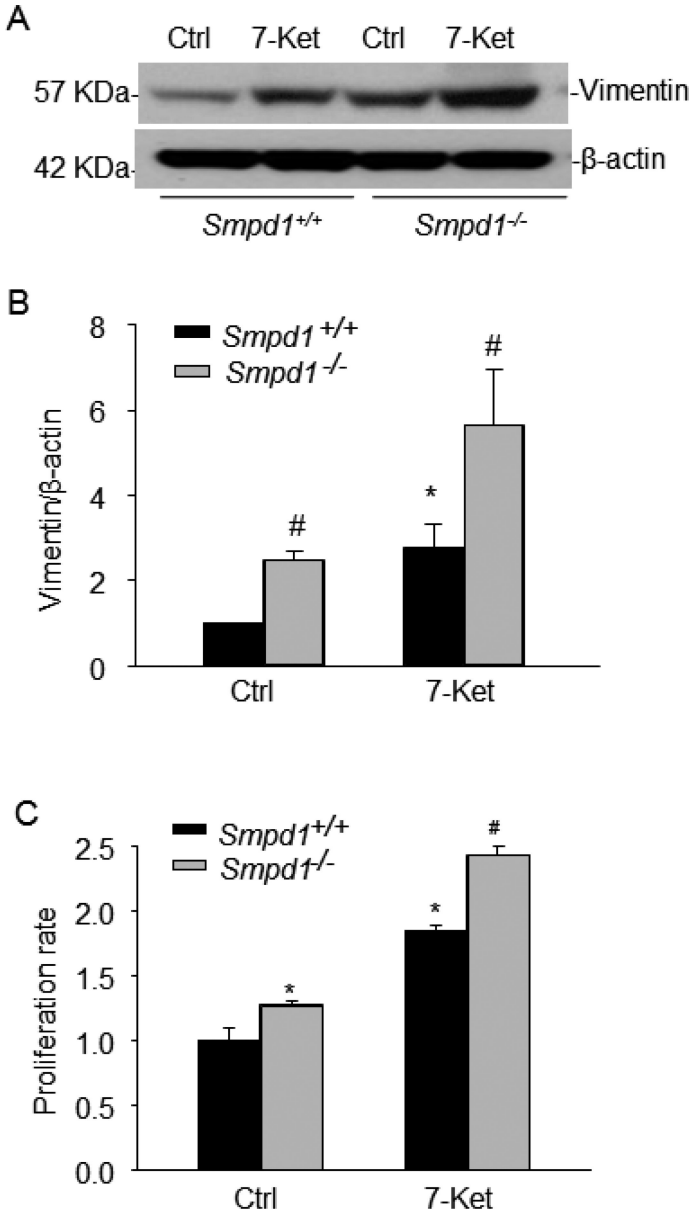

Figure 7. ASM deficiency enhances vimentin expression and cell proliferation in CASMCs upon atherogenic stimulation

Mouse CASMCs were either under control conditions or stimulated with 7-ketocholesterol (7-Ket, 10 μM) for 24 hours. (A) Representative Western blot gel documents and (B) summarized data showing the protein expression of vimentin and β-actin in *Smpd1*$^{+/+}$ or *Smpd1*$^{-/-}$ CASMCs (n=4). (C) Summarized data showing the relative proliferation rate of *Smpd1*$^{+/+}$ and *Smpd1*$^{-/-}$ CASMCs under control conditions or treated with 7-Ket (10 μM; 48 hours) (n=6). * P<0.05 *vs. Smpd1*$^{+/+}$ control; #*P* < 0.05 *Smpd1*$^{-/-}$ *vs. Smpd1*$^{+/+}$.

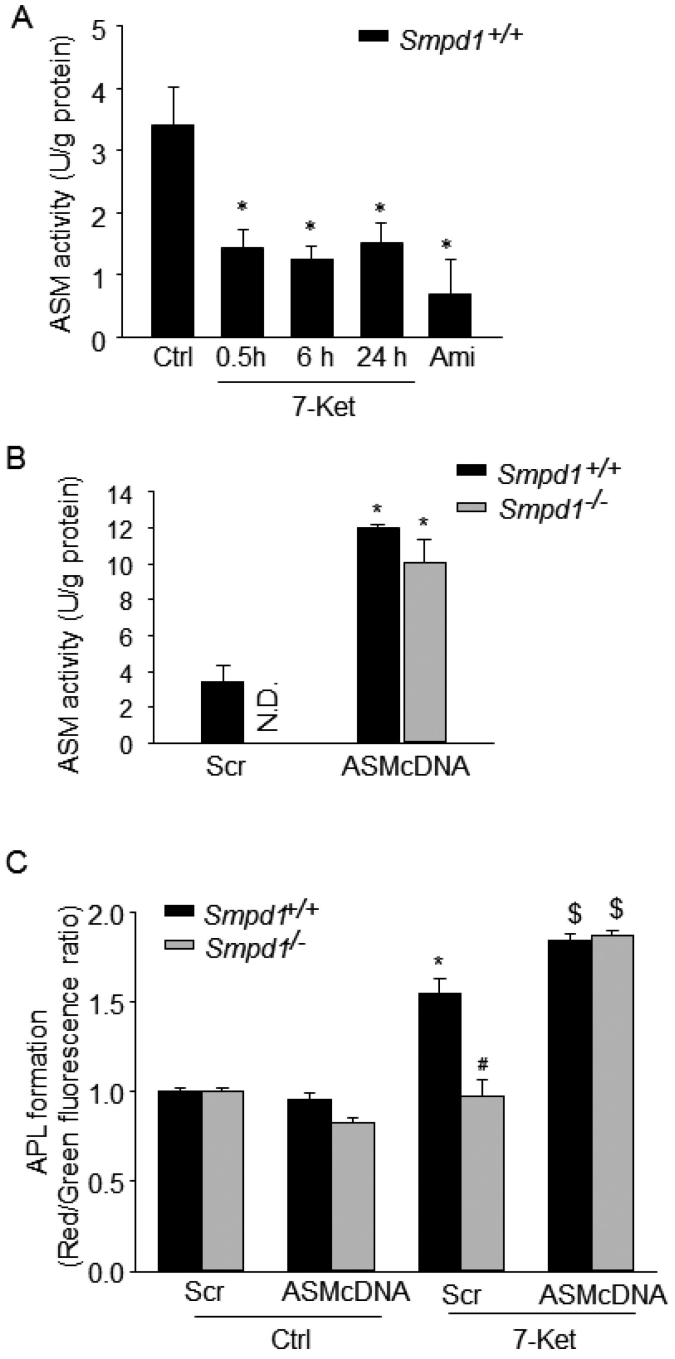

Figure 8. ASM overexpression increases autophagolysosomes (APLs) formation in CASMCs upon atherogenic stimulation

(A) Effects of 7-Ket (10 μM for 0.5, 6 or 24 hours) or amitriptyline (Ami; 10 μM for 24 hours) on ASM activity in *Smpd1*$^{+/+}$ CASMCs. (B) Mouse CASMCs were transfected with ASM cDNA plasmid encoding *Smpd1* gene or control vector with scrambled cDNA (Scr) by Nucleofection technology. Summarized data showing ASM activity in *Smpd1*$^{+/+}$ and *Smpd1*$^{-/-}$ CASMCs transfected with ASM cDNA plasmid or scramble. (C) Summarized red-to-green fluorescence ratio of acridine orange staining in ASM cDNA or scramble transfected *Smpd1*$^{+/+}$ or *Smpd1*$^{-/-}$ CASMCs under control condition or with atherogenic

stimulation by 7-Ket (10 μM; 24 hours). *P<0.05 *vs.* $Smpd1^{+/+}$ control; #$P < 0.05$ $Smpd1^{-/-}$ *vs.* $Smpd1^{+/+}$; $$P < 0.05$ *vs.* Scr+7-Ket (n=4).